Article

On a Novel Modulation Cutting Process for Potassium Dihydrogen Phosphate with an Increased Brittle–Ductile Transition Cutting Depth

Yang Yang *, Yu Chen and Chenyang Zhao *

School of Mechanical Engineering and Automation, Harbin Institute of Technology (Shenzhen), Shenzhen 518055, China
* Correspondence: yangyang2020@hit.edu.cn (Y.Y.); zhaochenyang@hit.edu.cn (C.Z.)

Abstract: Potassium dihydrogen phosphate (KDP) has garnered considerable attention due to its diverse applications across various scientific and engineering domains. Although promising machining performance enhancements have been achieved in ultra-precision diamond cutting, the brittle–ductile transition (BDT) depth for KDP crystals is essentially at the nanometer range and limits the further improvement of machining efficiency. In this paper, a novel ultra-precision diamond cutting process based on tool trapezoidal modulation is proposed for the first time to investigate the BDT characteristics of KDP crystals. By intentionally designing the tool modulation locus, the uncut chip thickness and cutting direction in the cutting duty cycle are kept constant, which provides a new strategy for probing the BDT mechanism and enhancing the machining performance. The BDT depth is significantly increased compared to the conventional ultra-precision diamond cutting owing to its unique modulation machining advantages. The significance of this paper lies not only in the improvement of the machining efficiency of KDP crystals through the proposed modulation cutting process, but also in the possibility of extending the relevant research methods and conclusions to the machining performance enhancement of other brittle optical crystals.

Keywords: KDP crystal; brittle–ductile transition; modulation cutting; anisotropic material; ultra-precision diamond cutting

Citation: Yang, Y.; Chen, Y.; Zhao, C. On a Novel Modulation Cutting Process for Potassium Dihydrogen Phosphate with an Increased Brittle–Ductile Transition Cutting Depth. *Machines* **2023**, *11*, 961. https://doi.org/10.3390/machines11100961

Academic Editor: Mark J. Jackson

Received: 18 September 2023
Revised: 11 October 2023
Accepted: 13 October 2023
Published: 16 October 2023

Copyright: © 2023 by the authors. Licensee MDPI, Basel, Switzerland. This article is an open access article distributed under the terms and conditions of the Creative Commons Attribution (CC BY) license (https://creativecommons.org/licenses/by/4.0/).

1. Introduction

Potassium dihydrogen phosphate (KDP) is a transparent optical crystal that is widely used as a frequency modulation device and an electro-optical switch for high-power lasers due to its excellent optical characteristics such as high nonlinear coefficients, a wide transmission bandwidth and a high laser damage threshold [1]. Serving as the only optical crystal suitable for inertial confinement nuclear fusion, large-aperture KDP plays an irreplaceable role in a series of scientific facilities such as the National Ignition Facility [2], Laser Megajoule [3] and SG-III Laser Facility [4]. However, the low hardness, high brittleness and strong anisotropy of KDP crystals cause severe challenges for the high-quality machining of KDP crystals. The undesired machining defects and brittle cracks on the machined surface and subsurface significantly deteriorate the working performance and lifetime of the corresponding components composed of KDP crystals [5–7]. Hence, ultra-precision machining is widely considered as an indispensable technique for generating high-quality KDP crystal components [8].

The mainstream ultra-precision machining methods for KDP crystals can be classified into ultra-precision abrasive machining and ultra-precision diamond cutting [9]. To tackle the surface deliquescence and abrasive inlaying problems in traditional abrasive machining, the newly developed magnetorheological finishing and non-corrosive particle jet polishing have been recently proposed to realize accurate anti-wetting threshold control and the dissolved material removal of KDP crystals [10,11]. Nevertheless, the intrinsic low material

removal efficiency and inflexibility of abrasive machining processes remain to be resolved, particularly for the machining of large-sized KDP crystals [12]. Additionally, the presence of distinct atomic arrangements and bonding strengths across varying crystallographic orientations introduces variations in mechanical properties. This microstructural diversity translates into disparate macroscopic mechanical attributes, manifesting as varying hardness and Young's modulus corresponding to different crystallographic directions [13–15].

On the other hand, ultra-precision single-point diamond cutting (SPDC) has received increasing attention in the use of KDP machining, evidenced by the continuously growing number of publications in the past few decades [16,17]. Actually, ductile-regime material removal and a crack-free machined surface can be achieved for brittle materials providing an actual cutting depth less than a critical value called the brittle–ductile transition (BDT) depth [18,19]. The BDT phenomenon has been widely identified in the ultra-precision diamond cutting of KDP crystals, whereas the BDT depth is reported to exhibit distinct anisotropy along the different crystal orientations and different crystal planes due to its anisotropic mechanical properties [20,21]. The ductile and brittle machining zones, hence, appeared alternatively on the machined surface during a diamond turning of KDP crystals [22]. In order to reveal its ductile material removal mechanism, theoretical models have been established to predict the critical cutting depth and load at the BDT cutting states [23,24]. A kinematic model and wavelet analysis method have been constructed to predict the surface roughness under various combinations of cutting process parameters by incorporating the ductile plasticity and brittle crack characteristics [25,26]. Building on the insights gained from the fundamental nano-indentation, the optimal ductile material removal with shallow subsurface damage was identified on the (001) plane [27]. In addition, an elevated temperature and large negative tool rake angles are favorable for increasing the fracture toughness and suppressing the crack propagation for achieving the nanometer surface roughness of KDP crystals [28–30]. Although promising machining performance enhancement has been achieved in the ultra-precision diamond cutting, the BDT depth for KDP crystals is essentially at the range of 80 nm–180 nm and limits the further improvement of machining efficiency [31]. Moreover, the micro-defects and brittle cracks left on the machined surfaces lead to the deterioration of the output laser beam quality and require a post-treatment process [32,33].

To enhance machining efficiency, researchers have recently developed the vibration-assisted machining technique by combining ultra-precision SPDC with vibration technology [34–36]. Compared to the conventional SPDC, this method can significantly reduce the cutting force and improve the BDT depth for brittle materials [37,38]. Zhang et al. achieved ultra-precision micro-grooves using vibration-assisted cutting on tungsten carbide and single-crystal silicon with a BDT depth over 12 times greater than that of the conventional SPDC method [39]. Huang et al. developed a vibration-assisted ductile machining model for KDP crystals by taking material properties and vibration parameters into account [40]. However, during the vibration-assisted machining of the KDP crystals, the uncut chip thickness and the magnitude and direction of cutting velocity continually vary along the vibration cutting cycle, resulting in a complex mechanism of the brittle-to-ductile transition.

In this paper, a novel ultra-precision diamond cutting process based on tool trapezoidal modulation is proposed for the first time to investigate the BDT characteristics of KDP crystals. By intentionally designing the tool modulation locus, the uncut chip thickness and cutting direction in the cutting duty cycle are kept constant, which provides a new strategy for probing the BDT mechanism and enhancing the machining performance. The BDT depth is significantly increased compared to the conventional ultra-precision single-point diamond cutting owing to its unique modulation machining advantages. The variation in the dynamic cutting force profile has been also investigated to explain the increase in BDT depth. The significance of this paper not only lies in the improvement of the machining efficiency of KDP crystals through the proposed modulation cutting process, but the relevant research methods and conclusions can also be extended to the machining performance enhancement of other brittle optical crystals.

2. Materials and Methods

2.1. KDP Crystal

As illustrated in Figure 1, KDP belongs to the tetragonal lattice system with a space group of $I42^d$. The high brittleness of KDP crystals essentially originates from the tetrahedron group $[PO4]1^{3-}$ and cations mainly connected by ionic bonds. The tested KDP crystal was sliced into a rectangular shape using a diamond wire saw with an overall size of 20 mm × 20 mm × 4 mm. Then, the KDP crystal was polished to obtain a damage-free surface with surface roughness (Ra) of less than 10 nm before the cutting processes. The machined surface corresponds to the (001) crystal plane of KDP, which has the tetragonal crystal system featuring unchanged mechanical properties after rotating 90° around its symmetrical optic axis. Hence, the KDP crystal will exhibit cutting anisotropy along the different cutting directions. In this study, the nominal cutting direction was set along the [110] crystal orientation of the (001) crystal plane. The mechanical properties of the KDP crystal are shown in Table 1.

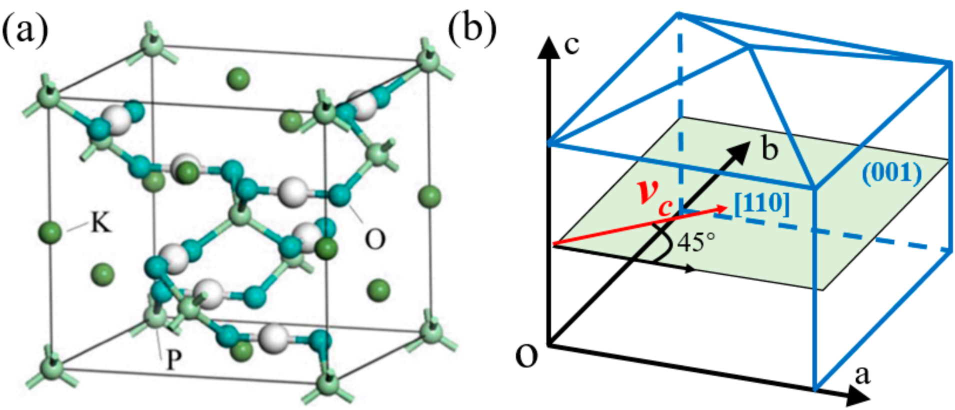

Figure 1. (**a**) Three-dimensional crystal structure of KDP [29] and (**b**) coordinate system showing (001) crystal plane as the machined surface (green area) and the nominal cutting direction (red arrow) along the crystal orientation [110].

Table 1. Material parameters for the employed KDP crystals.

Mechanical Property	Value	Mechanical Property	Value
Working surface	(001) crystal plane	Fracture toughness K_c	0.3 MPa $m^{1/2}$
Hardness H	2.0 GPa	Yield strength σ_s	51 MPa
Young's modulus E	44 GPa	Specific surface energy γ_s	0.6 J/m^2

2.2. Two-DOF Fast Tool Servo Mechanism

To generate the desired tool modulation locus, a piezoelectrically driven non-resonant fast tool servo mechanism was developed and manufactured from a spring steel monolithic piece by wire electrical discharge machining. As shown in Figure 2, the device was constructed using two symmetrical flexural limbs and an end-effector. Two piezoelectric stack actuators with an envelope size of 5 mm × 5 mm × 20 mm (PEA, Thorlabs PK4FTH3P2) were used to generate two-directional input displacements along the Y direction, which were amplified by the bridge-type displacement amplification mechanism (BDAM). Then, the amplified 2-DOF input displacement on the XOZ plane was delivered by a series of right circular flexure hinges (RCFHs) and bi-axis right circular flexure hinges (BRCFHs) and coupled onto the end-effector. The single-crystalline diamond cutting tool was screwed to the end-effector for executing the cutting operation. In addition, the graphical programming software LabVIEW was used to provide excitation voltages for the adopted PEAs through a multifunction I/O device and two power amplifiers (PX200). Two capacitance displacement sensors (Lion Precision CPL490) with a measuring resolution of 1 nm and a working bandwidth of 50 kHz were perpendicularly arranged to indirectly monitor the

tool position by measuring the output end displacements of BDAM, whose displacements were set as feedback signals to accomplish the closed-loop position control based on the calibrated displacement relationship between the output end of BDAM and the cutting tool. The classical PID control strategy was used to compensate the hysteresis effect of PEAs and overcome the cutting force to ensure the desired tool modulation locus. The arbitrary tool locus could be flexibly adjusted in a workspace of up to 26 µm along the *X*-axis direction and 15 µm along the *Z*-axis direction with an operating bandwidth of up to 4 kHz. The detailed trapezoidal generation procedures and locus accuracy analysis are elaborated in Section 3.1.

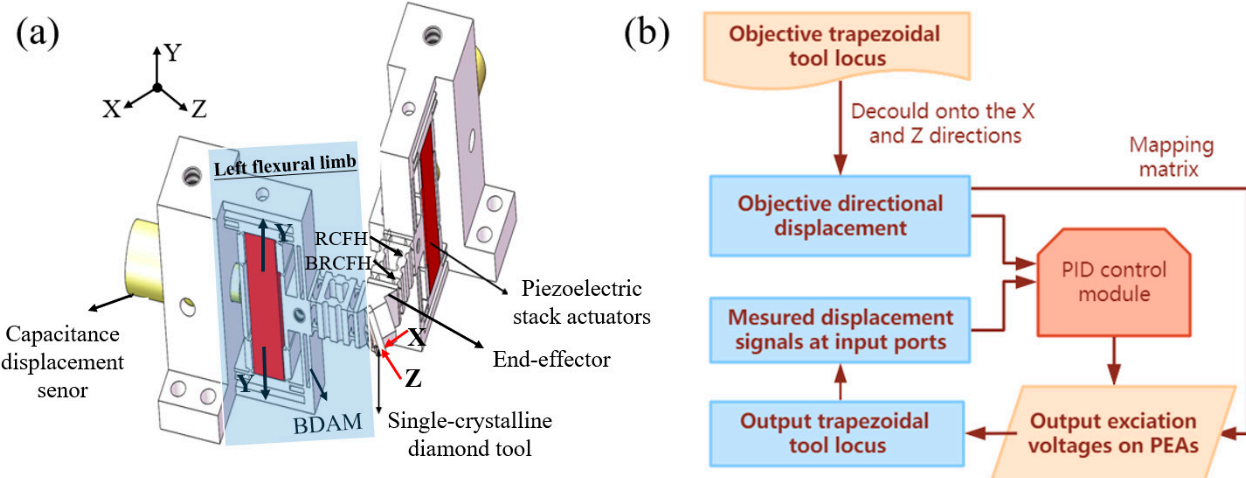

Figure 2. Two-DOF fast tool servo mechanism for trapezoidal tool locus generation. (**a**) Three-dimensional overview of servo mechanism; (**b**) process flow for generating the trapezoidal tool locus.

2.3. *Proposal of Novel Modulation Cutting Process*

The machining principle of the proposed novel modulation cutting (NMC) process is illustrated in Figure 3a. During the cutting process, the diamond tool is actuated to vibrate periodically along a two-dimensional trapezoidal locus on the cutting plane while the workpiece is fed rightward. It is noted that the ideal trapezoidal tool locus with four sharp corners will lead to non-smooth variations for the corresponding excitation voltage curves, which brings a series of ultra-high-frequency components far beyond the working bandwidth of the developed tool servo system. Hence, the ideal tool motion should be passed through a low-pass filter to obtain the achievable trapezoidal tool locus by setting the cut-off frequency as the system's working bandwidth [41]. An example of an excitation voltage curve for generating the filtered trapezoidal tool vibration and the excitation voltage curves corresponding to its four motion sides are marked as shown in Figure 3b. When the bottom side of the trapezoidal locus is set parallel to the nominal cutting direction, the diamond tool begins to cut into the KDP crystal at the bottom side of the trapezoidal locus. The instantaneous uncut chip thickness (UCT) quickly increases from zero to a local maximum value until the diamond tool reaches the secondary motion side. Then, the crystal material will be removed with a fixed UCT under unchanged cutting velocity and effective tool angles. Finally, the UCT will gradually decrease to zero when the tool arrives at the workpiece surface. The remaining distances on the secondary motion side as well as the third and fourth motion sides are the non-cutting duty cycle, where the diamond tool and crystal workpiece completely separate from each other. The above cutting process repeats during each tool vibration cycle.

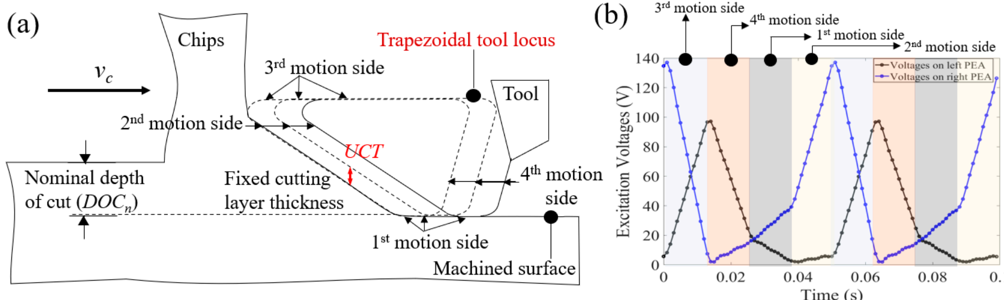

Figure 3. (**a**) Machining principle of proposed novel modulation cutting (NMC) process; (**b**) an example of excitation voltage curves on the left and right PEAs for generating trapezoidal tool vibration.

It is well known that the brittle KDP crystal can be removed in a ductile regime to generate a crack-free surface if the UCT is less than its BDT depth. For the proposed NMC process, the maximum UCT is achieved at the secondary side of the trapezoidal locus. Intuitively, the ductile material removal and crack-free surface can be realized by planning the process parameters to ensure the maximum UCT is less than BDT depth. Indeed, the material removal volume can be further enhanced by allowing certain crack propagation during the NMC process as the induced cracks do not penetrate into the final machined surface. The cracks induced in the previous vibration cutting cycle will be removed in the following vibration cutting cycles. This unique strategy of allowing an intermediate brittle mode of material removal, hence, contributes to a larger maximum allowable cutting depth without sacrificing the machining objective of obtaining a crack-free machined surface. In addition, the UCT and cutting direction at the secondary side of the duty cycle are constant values depending on the trapezoidal locus and nominal cutting velocity, which is independent of the nominal cutting depth. This unique feature provides a guideline for the optimal design of the tool trapezoidal locus to further enhance the machining performances.

2.4. Machining Setup and Surface Characterization

To investigate the feasibility of the proposed NMC process for KDP crystals, a set of micro-grooving plunge cutting experiments were carried out using a customized tri-axis ultra-precision machine center as shown in Figure 4. The KDP workpiece was first glued to an acrylic plate adaptor. Then, the inclined angle of the workpiece with respect to the nominal cutting direction was adjusted using a spacer to ensure the plunge cutting condition. The acrylic plate adaptor was screwed to a high-performance dynamometer (Kistler 9109AA), which is capable of accurately capturing the dynamic cutting force of the NMC process with a natural frequency of up to 15 kHz. The dynamometer was then attached to a tri-axis nano-positioning stage (Aerotech ANT 130) with a positioning resolution of 1 nm and a repeatability of 75 nm, which provided the primary cutting motion and the depth of cut with its X axis and Z axis, respectively. During the cutting process, a natural single-crystalline diamond (SCD) insert with a nose radius of 5.1 mm, a rake angle of -25° and a clearance angle of 20° was employed to execute the cutting operation under dry conditions. The tool edge profile was evaluated under an atomic force microscope (Bruker Dimension Icon AFM) to determine the cutting edge radius, which was around 150 nm. For comparison, the conventional single-point diamond cutting (SPDC) operation was also carried out by setting the objective tool locus as immobile. The nominal cutting velocities for the conventional SPDC and proposed NMC were kept the same at 2.4 mm/min. The overall machining parameters are summarized in Table 2. After the micro-grooving experiments, the machined KDP surfaces were coated with a platinum layer using ion sputtering equipment (HITACHI MC1000) in a vacuum condition. Then, the KDP crystals were studied under a scanning electron microscope (SEM, MDTC-EQ-M57-01) with a magnification ratio of 100.

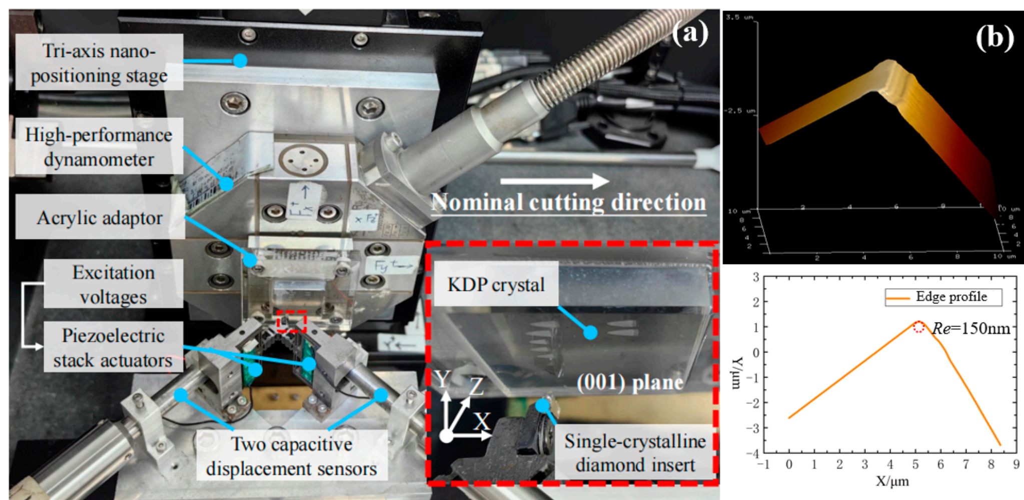

Figure 4. (**a**) Machining setup of the NMC process; (**b**) measurement of cutting edge radius.

Table 2. Summary of machining parameters.

Workpiece: (001) Crystal Plane of KDP		**Nominal Cutting Velocity v_c: 2.4 mm/min**	
Cutting tool parameters	Tool material: SCD Nose radius R_n: 5.1 mm Rake angle γ_0: $-25°$ Clearance angle α: 20°	Tool modulation locus parameters	Bottom length l: 3.5 μm Modulation height h: 2.2 μm First inclined angle θ: 75° Second inclined angle β: 75°

3. Results and Discussion

3.1. Generation of Trapezoidal Tool Motion Locus

As shown in Figure 5, the trapezoidal tool locus can be necessarily described by five parameters, namely the bottom length l, height h, first inclined angle θ, second inclined angle β and motion frequency f. To generate the desired trapezoidal tool locus before the cutting process, the developed 2-DOF fast tool servo is employed. Built on its working principle, the relationship between the imposed voltages and tool-tip displacement can be given by the following equations:

$$D_x(t) = k_{xl} \cdot V_L(t) - k_{xr} \cdot V_R(t) \tag{1}$$

$$D_z(t) = k_{zl} \cdot V_L(t) + k_{zr} \cdot V_R(t) \tag{2}$$

where D_x and D_z are the tool-tip displacements along the cutting and thrust directions; V_L and V_R are excitation voltages imposed on the left and right PEAs; and k_{xl}, k_{xr}, k_{zl} and k_{zr} are the constant coefficients and calibrated to be 0.0383 μm/V, 0.0823 μm/V, 0.0166 μm/V and 0.0209 μm/V, respectively. Then, based on these equations, an arbitrary trapezoidal tool locus can be realized by commanding the corresponding excitation voltages. As discussed earlier, the calculated excitation voltages for the non-harmonic trapezoidal locus will include the frequency components far beyond the working bandwidth of the developed tool servo system. To prevent the nonlinear response and ensure the accuracy of the trapezoidal locus generation, the tool motions along the cutting and thrust directions are expressed as a Fourier series. Consequently, a low-pass filter is utilized to obtain the achievable trapezoidal tool locus by setting the cut-off frequency as the system's working bandwidth. In addition, the closed-loop control strategy can be established by taking the real-time locus as a feedback signal for improving the motion generation accuracy and stability during the cutting process.

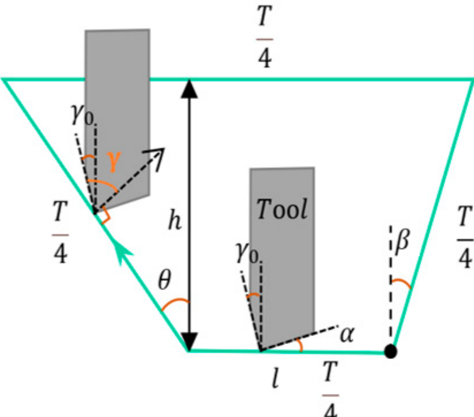

Figure 5. Mathematical representation of tool modulation locus. T represents the time periodicity of one trapezoidal vibration cycle.

A trapezoidal locus with a length l of 3.5 µm, height h of 2.2 µm, first inclined angle θ of 75°, second inclined angle β of 75° and motion periodicity of 50 ms is set as the objective trapezoidal locus. As illustrated in Figure 6, the non-harmonic motion trajectories along the cutting and thrust directions were generated and compared with the theoretical ones. It can be seen that good consistency can be identified under the closed-loop control. Root-mean-square errors less than 0.6 µm and 0.1 µm were identified for the tool motion along the cutting and thrust directions with motion strokes of up to twenty micrometers. The minor tracking errors were mainly attributed to the slight hysteresis property of PEAs and the parasitic motions of the employed servo mechanism.

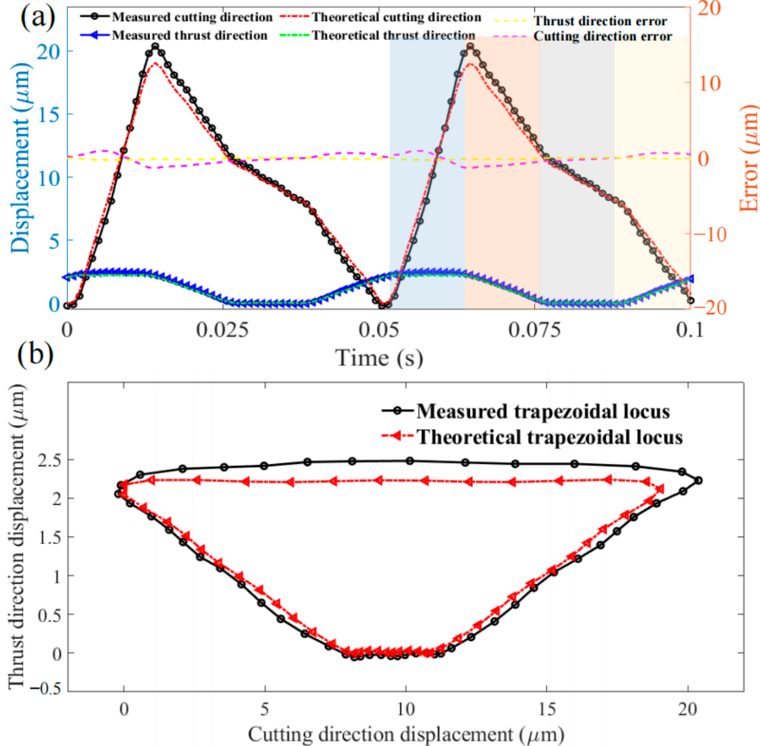

Figure 6. Generation of trapezoidal tool motion locus: (**a**) comparison of measured motion profile along the cutting and thrust directions with the theoretical results; (**b**) comparison of measured trapezoidal tool locus with the theoretical result.

3.2. Machined Surface Morphological Characterization

Two micro-grooving plunge cutting trials were carried out by commanding the servo mechanism to drive the cutting tool to be immobile and vibrate along the above trapezoidal locus. As the micrographs in Figure 7 show, the brittle–ductile transition can be clearly identified for the SPDC and NMC processes. The ductile and brittle machining regions exhibit completely different surface morphologies for the two machining processes. For the SPDC process, the ductile–brittle transition appears quickly after the initiation of the cutting operation with a cutting length, l_c, of around 25.6 μm. As indicated by the measured transition shoulder widths of w_c, the BDT depths (t_c) for the adopted cutting direction on the (001) crystal plane can be calculated to be around 169 nm, as illustrated in Figure 8. The identified result is consistent with the literature result on the 45° crystal orientation [31], which has the maximum BDT depth among all the possible crystal orientations on the (001) crystal plane. For comparison, the machined surfaces under the NMC process exhibit a brittle–ductile transition until the cutting length reaches 332 μm. The BDT depth was determined to be 4790 nm using the geometric relationship between the tool nose radius and the transition shoulder width. It can be deduced that an increment of more than 28 times in the BDT depth has been achieved by the proposed NMC process, which is highly beneficial for the high-efficiency machining of KDP crystals in the ductile regime. In addition, the surface roughness Ra is identified to be 7 nm and 17 nm under the AFM inspections for the ductile machined regions of the SPDC and NMC processes, respectively. The similar surface roughness values further confirm the feasibility and superiority of the proposed NMC process as it can achieve ductile-regime machining of KDP crystals under a much larger cutting depth.

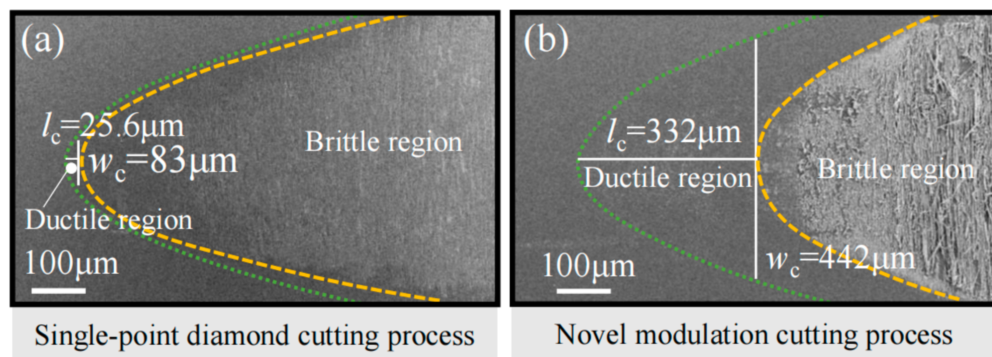

Figure 7. SEM micrographs of machined surfaces under (**a**) the conventional single-point diamond cutting process and (**b**) the proposed novel modulation cutting process.

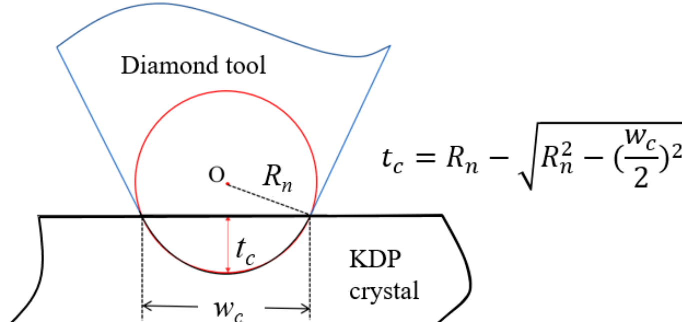

Figure 8. Relationship between the transition shoulder width and the BDT depth.

In the meantime, it can also be seen that the machined brittle regions under the NMC process are quite different from those of the conventional SPDC process. Obvious crystal cracks and brittle fractures are pervasive on the machined surface, which is attributed to the dynamic cutting attribute of the proposed NMC process. In the brittle-regime cutting state

with segmented chips, the periodic contact between the tool and KDP workpiece not only alters the intrinsic chip formation but also changes the machining stability of the dynamic cutting. Undesired machining chatters and tool locus fluctuation further complicate the material removal mechanism compared to the conventional SPDC process. Therefore, the cutting depth should be strictly controlled under the BDT depth for the proposed NMC process to prevent the possible material removal state from turning into the brittle regime.

3.3. Cutting Force Analysis

To investigate the material removal mechanism, the cutting force profiles for the conventional SPDC and the proposed NMC were collected and compared with each other. As illustrated in Figure 9a, the magnitudes of the thrust cutting force and main cutting force are similar and gradually increase during the conventional diamond cutting process due to the plunge cutting configuration. The cutting force signals experience a sudden increase in the initial cutting state, which is due to the material removal state shifting from the ductile regime to the brittle regime. Such a sudden increase in cutting force is consistent with the micrographs of the BDT discussed above. After that, significant high-frequency fluctuations in cutting force can be clearly observed with the gradually increased depth of cut. This is probably attributed to the increased proportion of the brittle fracture component in the cutting force, where the accumulated stress is released as crack formation occurs [42]. The magnitude of the thrust cutting force gradually exceeds the magnitude of the main cutting force despite a force fluctuation magnitude of around 300 mN. For comparison, the cutting force profile for the proposed trapezoidal modulation cutting shows highly dynamic characteristics during the micro-grooving cutting process. Moreover, it can be seen that the increasing rate of maximum force magnitude is much slower than that of the conventional SPDC process. This can be explained by the periodic contact and separation between the cutting tool and the KDP crystal. Consequently, the cutting force magnitudes are in general much smaller than those of SPDC under identical depths of cut. It is noted that the negative value of the measured cutting force might be partially attributed to the slight measurement errors under the dynamic cutting process due to the limited working bandwidth and the time-dependent drift of the employed dynamometer.

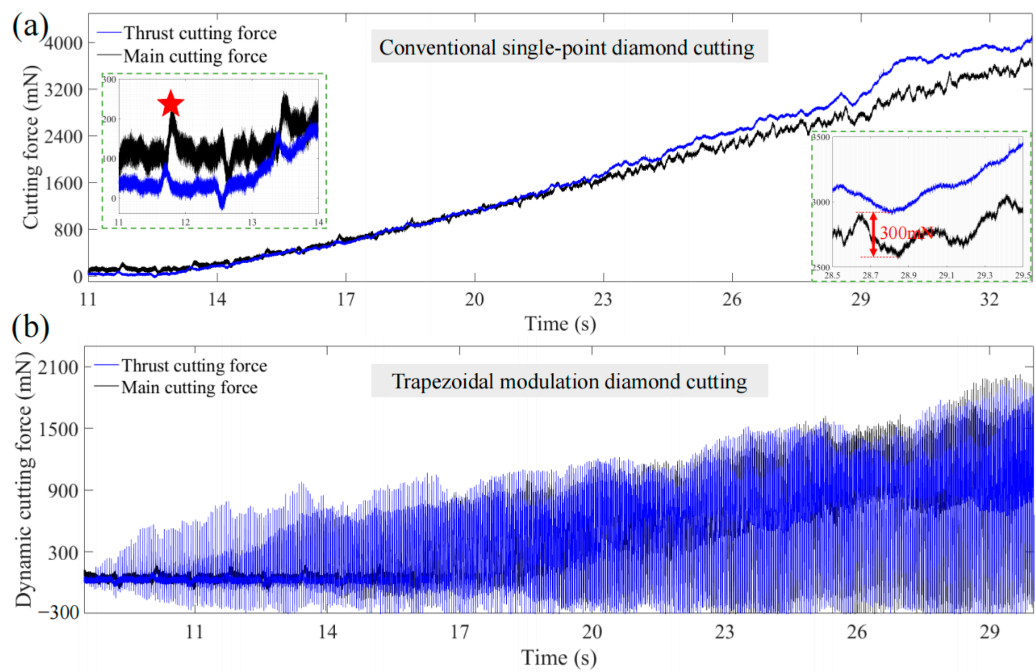

Figure 9. Overall comparison of cutting force variation trend during the taper cutting. (**a**) Conventional single-point diamond cutting; (**b**) proposed novel modulation cutting.

In order to clarify the dynamic attribute of cutting force in the proposed NMC process, three significant cutting durations are enlarged and shown in Figure 10. As can be seen, the periodic variation in cutting force can be clearly identified in the initial cutting duration. The modulation frequency is consistent with a tool motion frequency of 20 Hz. For the initial cutting with a depth of cut less than the height of the tool modulation locus, the cutting force magnitude gradually increases with the cutting depth but has an extremely low duty cycle ratio of cutting force as highlighted as Δt_1 in Figure 10a. When the cutting depth increases to the values near the trapezoidal height, the cutting duty cycle ratio tends to a constant value of Δt_2 determined by the kinematic relationship of the resultant cutting locus. During this state, the cutting tool maintains periodic contact and separation with the KDP crystal, and the main cutting duty lies on the secondary sides of the tool modulation locus. Hence, the variation in cutting force magnitude can be directly linked to the modulation of cutting load on the tool rake face, as the instantaneous UCT, cutting velocity and tool effective angles were kept unchanged. As the objective application of the proposed NMC process is the ultra-precision cutting of KDP crystals in the ductile regime with an increased BDT depth, several hundred millinewtons of cutting force with an extremely short duty cycle in the ductile regime is beneficial for preventing the tool wear and increasing the lifetime of diamond tools [43]. However, when the UCT further increases to the brittle regime, the dynamic cutting force profile exhibits completely different features, as shown in Figure 10c. Despite the identical modulation frequency of cutting force, the cutting duty cycle is nearly approaching 1. This can be explained by the material removal state in an almost completely brittle regime. The cutting force is then dominated by the formation of micro-cracks and brittle chips. A large amount of particle chips will randomly touch the modulated cutting tool, even under the non-cutting duty cycle, which leads to an increase in the duty cycle ratio and even negative values of the measured dynamic cutting force. Nevertheless, more comprehensive evaluations for the newly proposed NMC process still need to be carried out to further clarify other machining performances and compare them to the existing machining methods.

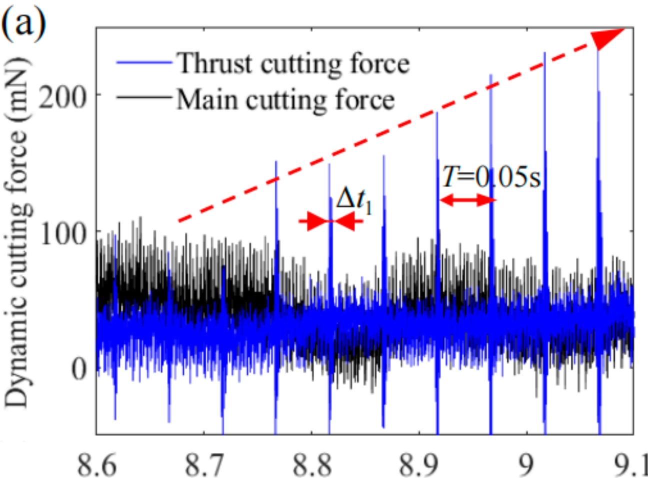

Figure 10. *Cont.*

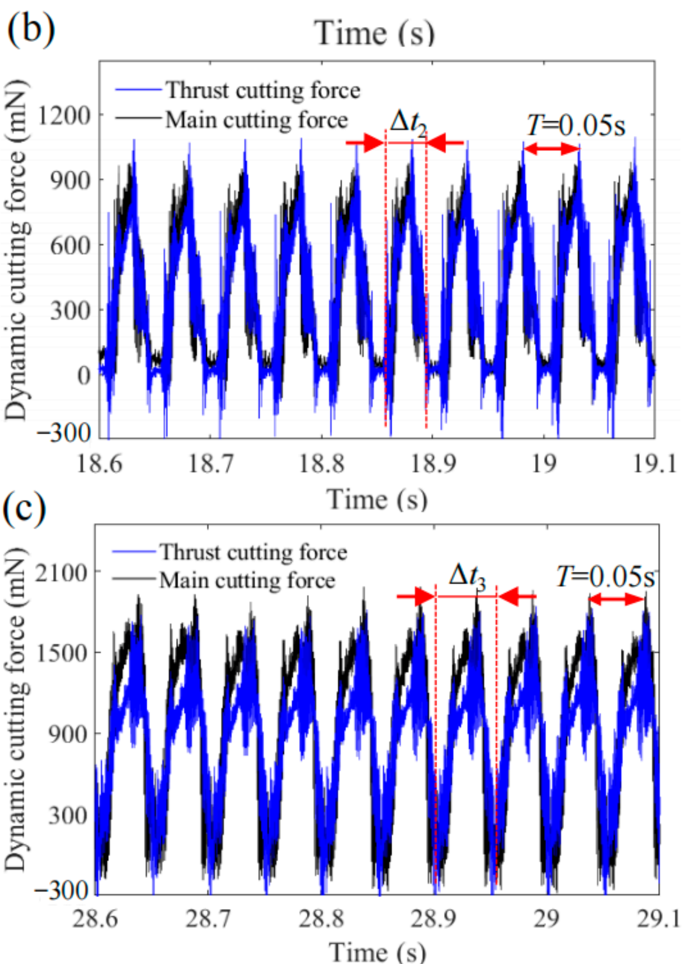

Figure 10. Dynamic cutting force process of trapezoidal modulation cutting. (**a**) Initial ductile-regime cutting; (**b**) stable ductile cutting duration; (**c**) brittle-regime cutting duration.

4. Conclusions

In this paper, a novel ultra-precision cutting process based on tool modulation was proposed for the ductile-regime machining of KDP crystals. The tool trapezoidal modulation locus was generated by a newly developed non-resonant fast tool servo mechanism, and the generation procedures and locus generation accuracy were analyzed. Then, the process principle of the NMC process was clarified, where the uncut chip thickness and cutting direction were kept as constant values, which is beneficial for ensuring a stable dynamic cutting process for brittle crystals. The brittle–ductile transition cutting depth was therefore significantly increased compared with conventional single-point diamond cutting. To investigate the material removal mechanism, the dynamic cutting forces for the NMC and the conventional SPDC process were systematically compared. It was found that the dynamic cutting force for the proposed NMC process is much smaller than that of SPDC and shows a much slower increase in the rate of maximum force magnitude due to the modulation cutting advantage. In addition, the modulation frequency of the dynamic cutting force is consistent with the tool motion frequency. The duty cycle ratio of cutting force is extremely low at the initial ductile cutting regime, then tending to a constant value and finally approaching 1. The underlying mechanism for the variation in the duty cycle ratio of cutting force was discussed and analyzed.

Author Contributions: Conceptualization, Y.Y.; methodology, Y.Y. and Y.C.; software, Y.C.; validation, Y.C. and Y.Y.; formal analysis, Y.C.; investigation, Y.C.; resources, C.Z.; data curation, Y.Y.; writing—original draft preparation, Y.Y.; writing—review and editing, Y.Y. and C.Z.; visualization, Y.Y.; supervision, Y.Y. and C.Z.; project administration, C.Z.; funding acquisition, Y.Y. All authors have read and agreed to the published version of the manuscript.

Funding: This research was funded by the Basic and Applied Basic Research Foundation of Guangdong Province with grant number 2020A1515110351 and Shenzhen Stable Support Grant with grant number GXWD20220811152145004.

Data Availability Statement: The data presented in this study are available on request from the corresponding author.

Conflicts of Interest: The authors declare no conflict of interest.

References

1. Chen, M.; Pang, Q.; Wang, J.; Cheng, K. Analysis of 3D microtopography in machined KDP crystal surfaces based on fractal and wavelet methods. *Int. J. Mach. Tools Manuf.* **2008**, *48*, 905–913. [CrossRef]
2. Baisden, P.; Atherton, L.; Hawley, R.; Land, T.; Menapace, J.; Miller, P.; Runkel, M.; Spaeth, M.; Stolz, C.; Suratwala, T. Large optics for the national ignition facility. *Fusion Sci. Technol.* **2016**, *69*, 295–351. [CrossRef]
3. Reyné, S.; Duchateau, G.; Natoli, J.-Y.; Lamaignère, L. Laser-induced damage of KDP crystals by 1ω nanosecond pulses: Influence of crystal orientation. *Opt. Express* **2009**, *17*, 21652–21665. [CrossRef] [PubMed]
4. Zhang, R.; Jia, H.; Geng, Y.; Li, P.; Liu, L.; Tian, X.; Yuan, H.; Fan, C.; Su, J.; Hu, D. Research of target uniform illumination on SG-III laser facility. In Proceedings of the High Power Lasers, High Energy Lasers, and Silicon-Based Photonic Integration, Beijing, China, 9–11 May 2016.
5. Cheng, J.; Wang, J.; Peng, E.; Yang, H.; Chen, H.; Chen, M.; Tan, J. Combined modulation of incident laser light by multiple surface scratches and their effects on the laser damage properties of KH_2PO_4 crystal. *Opt. Express* **2020**, *28*, 8764–8782. [CrossRef]
6. Qu, M.; Xie, G.; Jin, T.; Cai, R.; Lu, A. Realization of high efficiency and low damage machining of anisotropic KDP crystal by grinding. *Precis. Eng.* **2019**, *55*, 464–473. [CrossRef]
7. Hou, N.; Zhang, Y.; Zhang, L.; Zhang, F. Assessing microstructure changes in potassium dihydrogen phosphate crystals induced by mechanical stresses. *Scr. Mater.* **2016**, *113*, 48–50. [CrossRef]
8. Li, C.; Piao, Y.; Hu, Y.; Wei, Z.; Li, L.; Zhang, F. Modelling and experimental investigation of temperature field during fly-cutting of KDP crystals. *Int. J. Mech. Sci.* **2021**, *210*, 106751. [CrossRef]
9. Chen, W.; Liang, Y.; Sun, Y.; Huo, D.; Lu, L.; Liu, H. Design philosophy of an ultra-precision fly cutting machine tool for KDP crystal machining and its implementation on the structure design. *Int. J. Adv. Manuf. Technol.* **2014**, *70*, 429–438. [CrossRef]
10. Yin, Y.; Zhang, Y.; Dai, Y.; Xiao, Q.; Tie, G. Novel magneto-rheological finishing process of KDP crystal by controlling fluid-crystal temperature difference to restrain deliquescence. *CIRP Ann.* **2018**, *67*, 587–590. [CrossRef]
11. Gao, W.; Wei, Q.; Ji, J.; Sun, P.; Ji, F.; Wang, C.; Xu, M. Theoretical modeling and analysis of material removal characteristics for KDP crystal in abrasive-free jet processing. *Opt. Express* **2019**, *27*, 6268–6282. [CrossRef]
12. Cheng, Z.; Gao, H.; Liu, Z.; Guo, D. Investigation of the trajectory uniformity in water dissolution ultraprecision continuous polishing of large-sized KDP crystal. *Int. J. Extrem. Manuf.* **2020**, *4*, 045101. [CrossRef]
13. Wang, S.; An, C.; Zhang, F.; Wang, J.; Lei, X.; Zhang, J. Simulation research on the anisotropic cutting mechanism of KDP crystal using a new constitutive model. *Mach. Sci. Technol.* **2017**, *21*, 202–222. [CrossRef]
14. Jia, H.; Wang, F.; Wu, J.; Tan, X.; Cao, Y. Elastic properties and electronic structure of tetragonal KDP crystal under polishing pressures from first principles. *Int. J. Mod. Phys. B* **2020**, *34*, 2050286. [CrossRef]
15. Borc, J.; Sangwal, K.; Pritula, I.; Dolzhenkova, E. Investigation of pop-in events and indentation size effect on the (001) and (100) faces of KDP crystals by nanoindentation deformation. *Mater. Sci. Eng. A* **2017**, *708*, 1–10. [CrossRef]
16. Hou, N.; Zhang, L.; Zhang, Y.; Zhang, F. On the ultra-precision fabrication of damage-free optical KDP components: Mechanisms and problems. *Crit. Rev. Solid State Mater. Sci.* **2019**, *44*, 283–297. [CrossRef]
17. Huang, W.; Yan, J. Effect of tool geometry on ultraprecision machining of soft-brittle materials: A comprehensive review. *Int. J. Extrem. Manuf.* **2022**, *5*, 012003. [CrossRef]
18. Zhang, X.; Arif, M.; Liu, K.; Kumar, A.S.; Rahman, M. A model to predict the critical undeformed chip thickness in vibration-assisted machining of brittle materials. *Int. J. Mach. Tools Manuf.* **2013**, *69*, 57–66. [CrossRef]
19. Liu, Q.; Liao, Z.; Cheng, J.; Xu, D.; Chen, M. Mechanism of chip formation and surface-defects in orthogonal cutting of soft-brittle potassium dihydrogen phosphate crystals. *Mater. Des.* **2021**, *198*, 109327. [CrossRef]
20. Tie, G.; Dai, Y.; Guan, C.; Zhu, D.; Song, B. Research on full-aperture ductile cutting of KDP crystals using spiral turning technique. *J. Mater. Process. Technol.* **2013**, *213*, 2137–2144. [CrossRef]
21. Huang, W.; Yan, J. Fundamental investigation of diamond cutting of micro V-shaped grooves on a polycrystalline soft-brittle material. *J. Manuf. Mater. Process.* **2021**, *5*, 17. [CrossRef]

22. Chen, H.; Dai, Y.; Zheng, Z.; Gao, H.; Li, X. Effect of crystallographic orientation on cutting forces and surface finish in ductile cutting of KDP crystals. *Mach. Sci. Technol.* **2011**, *15*, 231–242. [CrossRef]
23. Zhao, Q.; Wang, Y.; Yu, G.; Dong, S.; Zhang, X. Investigation of anisotropic mechanisms in ultra-precision diamond machining of KDP crystal. *J. Mater. Process. Technol.* **2009**, *209*, 4169–4177. [CrossRef]
24. Li, C.; Zhang, Y.; Zhou, G.; Wei, Z.; Zhang, L. Theoretical modelling of brittle-to-ductile transition load of KDP crystals on (001) plane during nanoindentation and nanoscratch tests. *J. Mater. Res. Technol.* **2020**, *9*, 14142–14157. [CrossRef]
25. Wang, H.; Zong, W.; Sun, T.; Liu, Q. Modification of three dimensional topography of the machined KDP crystal surface using wavelet analysis method. *Appl. Surf. Sci.* **2010**, *256*, 5061–5068. [CrossRef]
26. Zhang, S.; Zong, W. A novel surface roughness model for potassium dihydrogen phosphate (KDP) crystal in oblique diamond turning. *Int. J. Mech. Sci.* **2020**, *173*, 105462. [CrossRef]
27. Yang, S.; Zhang, L.; Wu, Z. Effect of Anisotropy of Potassium Dihydrogen Phosphate Crystals on Its Deformation Mechanisms Subjected to Nanoindentation. *ACS Appl. Mater. Interfaces* **2021**, *13*, 41351–41360. [CrossRef]
28. Liu, Q.; Chen, M.; Liao, Z.; Feng, J.; Xu, D.; Cheng, J. On the improvement of the ductile removal ability of brittle KDP crystal via temperature effect. *Ceram. Int.* **2021**, *47*, 33127–33139. [CrossRef]
29. Liu, Q.; Liao, Z.; Axinte, D. Temperature effect on the material removal mechanism of soft-brittle crystals at nano/micron scale. *Int. J. Mach. Tools Manuf.* **2020**, *159*, 103620. [CrossRef]
30. Zhang, S.; Zhang, H.; Zong, W. Modeling and simulation on the effect of tool rake angle in diamond turning of KDP crystal. *J. Mater. Process. Technol.* **2019**, *273*, 116259. [CrossRef]
31. Wang, S.; An, C.; Zhang, F.; Wang, J.; Lei, X.; Zhang, J. An experimental and theoretical investigation on the brittle ductile transition and cutting force anisotropy in cutting KDP crystal. *Int. J. Mach. Tools Manuf.* **2016**, *106*, 98–108. [CrossRef]
32. Pritula, I.; Kolybayeva, M.; Salo, V.; Puzikov, V. Defects of large-size KDP single crystals and their influence on degradation of the optical properties. *Opt. Mater.* **2007**, *30*, 98–100. [CrossRef]
33. Zhang, H.; Zhang, X.; Li, Z.; Wang, P.; Guo, Z. Removing single-point diamond turning marks using form-preserving active fluid jet polishing. *Precis. Eng.* **2022**, *76*, 237–254. [CrossRef]
34. Yang, Y.; Gao, S.; Chen, K.; Pan, Y.; Guo, P. Vibration analysis and development of an ultrasonic elliptical vibration tool based on a portal frame structure. *Precis. Eng.* **2017**, *50*, 421–432. [CrossRef]
35. Yang, Y.; Wu, K.; Xiang, J. Numerical investigations on the dynamic ploughing interaction in elliptical vibration cutting. In Proceedings of the Second International Conference on Advanced Manufacturing Technology and Manufacturing Systems (ICAMTMS 2023), Nanjing, China, 26–28 May 2023.
36. Holthusen, A.-K.; Riemer, O.; Brinksmeier, E. Material impact on diamond machining of diffractive optical structures for UV-application. *J. Manuf. Mater. Process.* **2018**, *2*, 15. [CrossRef]
37. Zhou, M.; Wang, X.; Ngoi, B.; Gan, J. Brittle–ductile transition in the diamond cutting of glasses with the aid of ultrasonic vibration. *J. Mater. Process. Technol.* **2002**, *121*, 243–251. [CrossRef]
38. Fernando, P.; Zhang, M.; Pei, Z.; Cong, W. Intermittent and continuous rotary ultrasonic machining of K9 glass: An experimental investigation. *J. Manuf. Mater. Process.* **2017**, *1*, 20. [CrossRef]
39. Zhang, J.; Suzuki, N.; Wang, Y.; Shamoto, E. Fundamental investigation of ultra-precision ductile machining of tungsten carbide by applying elliptical vibration cutting with single crystal diamond. *J. Mater. Process. Technol.* **2014**, *214*, 2644–2659. [CrossRef]
40. Huang, W.; Yu, D.; Zhang, X.; Zhang, M.; Chen, D. Ductile-regime machining model for ultrasonic elliptical vibration cutting of brittle materials. *J. Manuf. Process.* **2018**, *36*, 68–76. [CrossRef]
41. Yang, Y.; Wen, J.; Zhang, Y. Development of a novel XZ workpiece vibration generator for cooperative vibration cutting of hierarchical grating structures. *Mech. Syst. Sig. Process.* **2023**, *198*, 110422. [CrossRef]
42. Huang, W.; Yu, D.; Zhang, M.; Cao, Q.; Yao, J. Predictive cutting force model for ductile-regime machining of brittle materials. *Int. J. Adv. Manuf. Technol.* **2018**, *98*, 781–790. [CrossRef]
43. Yang, Y.; Xiang, J.; Zhao, Z. An analytical cutting force model for elliptical vibration texturing of nano-grating surfaces. *J. Mater. Process. Technol.* **2023**, *315*, 117901. [CrossRef]

Disclaimer/Publisher's Note: The statements, opinions and data contained in all publications are solely those of the individual author(s) and contributor(s) and not of MDPI and/or the editor(s). MDPI and/or the editor(s) disclaim responsibility for any injury to people or property resulting from any ideas, methods, instructions or products referred to in the content.